DNA Y structure: a versatile, multidimensional single molecule assay

James T. Inman[1], Benjamin Y. Smith[1,2,†], Michael A. Hall[1,2,†], Robert A. Forties[1,2], Jing Jin[1,2,†],

James P. Sethna[1], Michelle D. Wang[1,2,]*

[1]Department of Physics, LASSP, Cornell University, Ithaca, NY 14853.

[2]Howard Hughes Medical Institute, Cornell University, Ithaca, NY 14853.

Supporting Information Discussion:

Supporting Information References

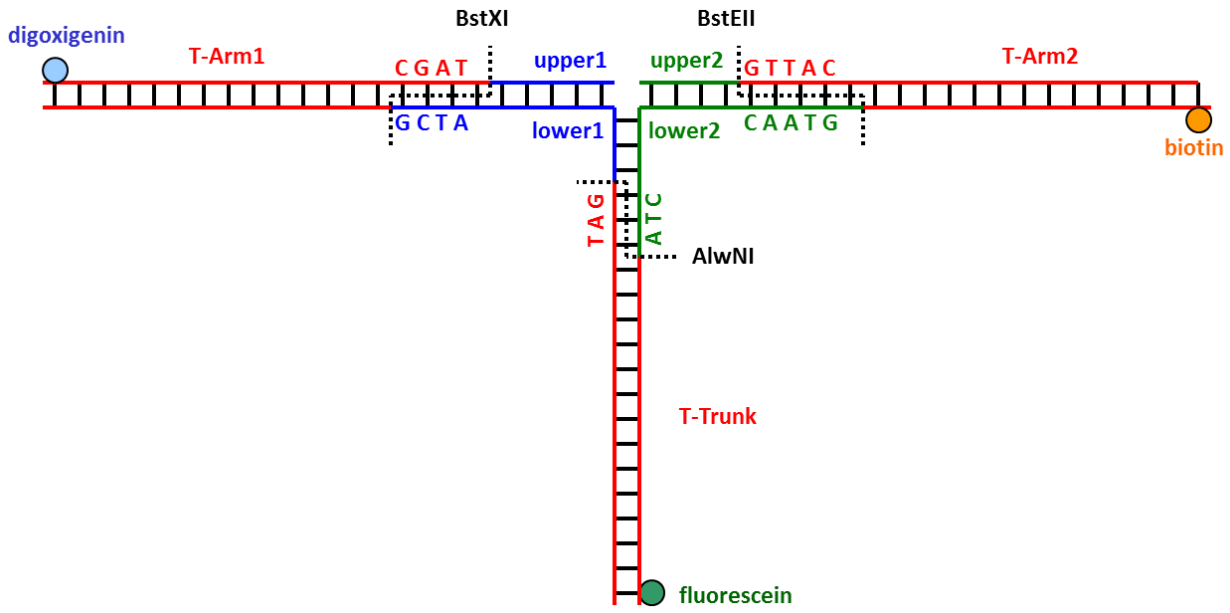

Figure S1. Construction of the Y structure. (1) Arm 1 DNA was cut from plasmid pMDW38 (sequence available upon request) and its 5' end was labeled with digoxigenin with a Klenow reaction. (2) Upper 1 (5'-/phos/GCA GTA CCG AGC TCA TCC AAT TCT ACA TGC CGC)and lower 1 (5'-/phos/GCC TTG CAC GTG ATT ACG AGA TAT CGA TGA TTG CG GCG GCA TGT AGA ATT GGA TGA GCT CGG TAC TGC ATC G) were annealed to form adapter 1. (3) Adapter 1 was ligated to arm 1 and the product was gel purified to remove un-ligated adapters. (4) Steps 1-3 were repeated for arm 2: upper 1 (5'-CGT TAC GTC ATT CTA TAC ACT GTA CAG) and lower 2 (5'-/phos/GTAAC CTG TAC AGT GTA TAG AAT GAC GTA ACG CGC AAT CAT CGA TAT CTC GTA ATC ACG TGC AAG GC CTA). (5) Arm 1 and arm 2 were annealed via lower 1 and lower 2. (6) Trunk DNA was prepared by PCR from pMDW2 (sequence available upon request) using a 5' fluorescein tag on one of the primers. (7) Arms were ligated to trunk DNA.

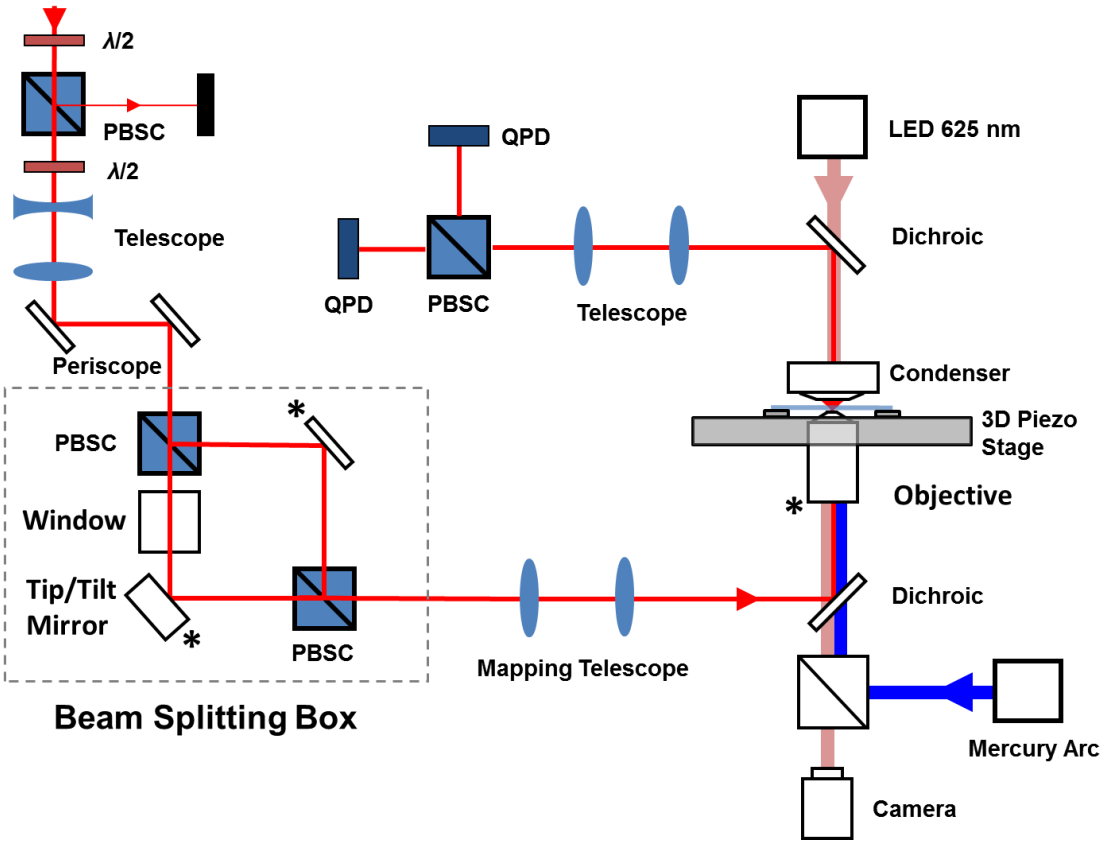

Figure S2. A dual optical trap setup with bright field and fluorescence illumination. A 1064-nm Gaussian trapping beam is coupled to a polarization maintaining single mode fiber (not shown). After collimation, the beam is sent through a half-wave plate and beam splitter that controls the input power and ensures that the beam is linearly polarized. A second half-wave plate rotates the polarization and this partitions the power in the dual trap. The beam is re-collimated to ~ 5 mm by an expansion telescope and elevated to the proper height by a periscope. To form the dual trap, the single Gaussian laser beam is split into two orthogonally polarized beams by a polarizing beam splitting cube (PBSC) in the 'Beam Splitting Box'. One beam is reflected off of a mirror that is mounted on a tip/tilt piezo. This mirror is mapped to the back focal plane of the objective such that it controls Trap 1's position while Trap 2 remains

fixed. The two beams are recombined by a second PBSC and expanded to ~ 10 mm by the mapping telescope. They are introduced into a Nikon TE200 microscope's imaging path and later to the trapping plane by a dichroic mirror. Upon exiting the condenser, the laser beams are reflected by a second dichroic mirror and again split by a PBSC. Each beam is detected by a quadrant photodiode (QPD). Bright field illumination is accomplished by 625-nm LED light introduced through the condenser lens. This light passes through the laser dichroic and the fluorescence cube set and is imaged by a cooled CCD. Fluorescence illumination is produced by a mercury arc lamp. The light is filtered and introduced into the illumination path by a fluorescence filter set optimized for quantum dots (excitation 350-450 nm, emission 625 nm).

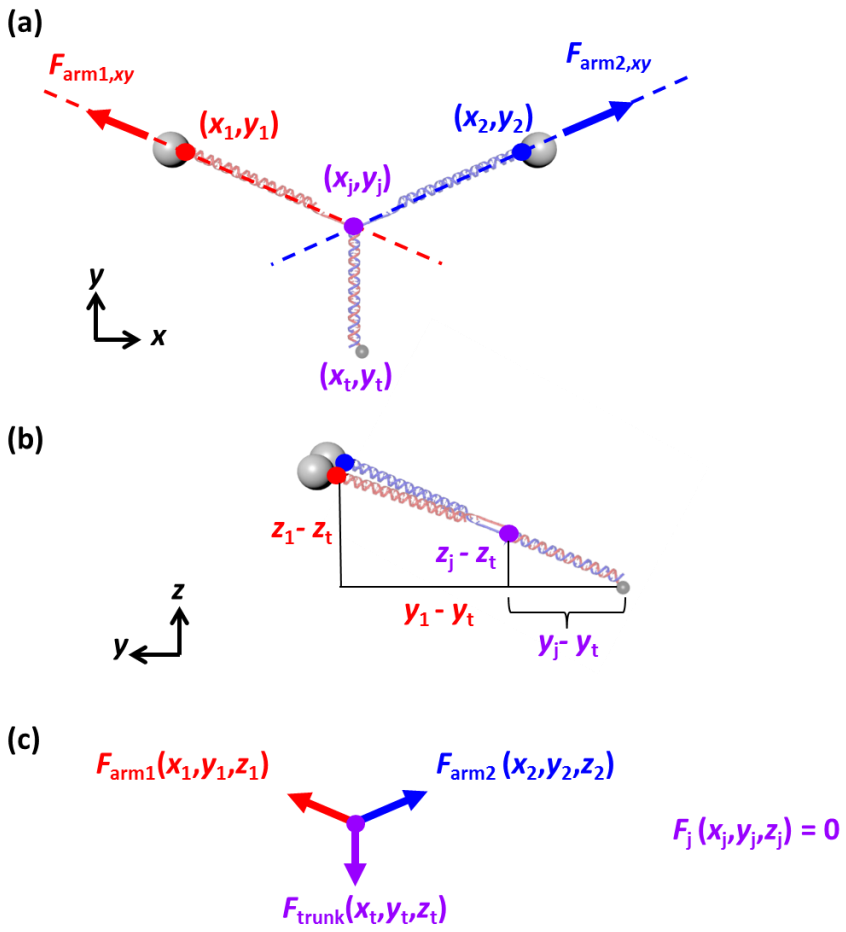

Figure S3. Calculation of Y structure forces and extensions.

(a) The projection of the Y structure onto the *xy* plane. The *xy* position of the Y junction is determined by the force and location of the trapped beads.

(b) The *z* location of the junction is determined by geometry.

(c) The forces are required to sum to zero at the junction.

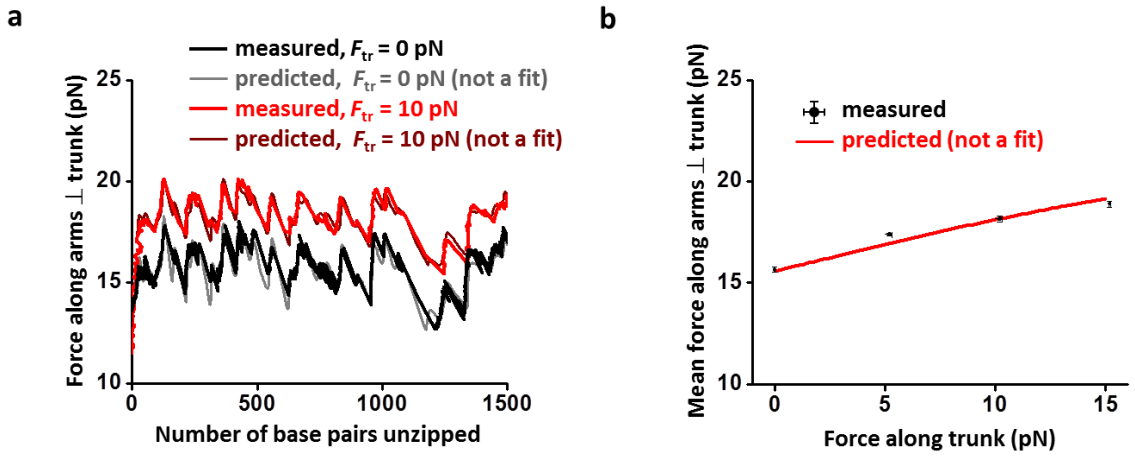

Figure S4. Component of force along arms perpendicular to trunk. The Y structure was unzipped under a constant trunk force.

(**a**) Component of force along arms perpendicular to the trunk versus number of base pairs unzipped under no trunk force (black) and 10 pN trunk force (red). Theoretical predictions are shown for comparison.

(**b**) Component of mean force along arms perpendicular to the trunk versus force along trunk (black). For each trunk force, component of the force along arms perpendicular to the trunk was averaged over the first 1500 bp unzipped. Theoretical prediction is shown in red.

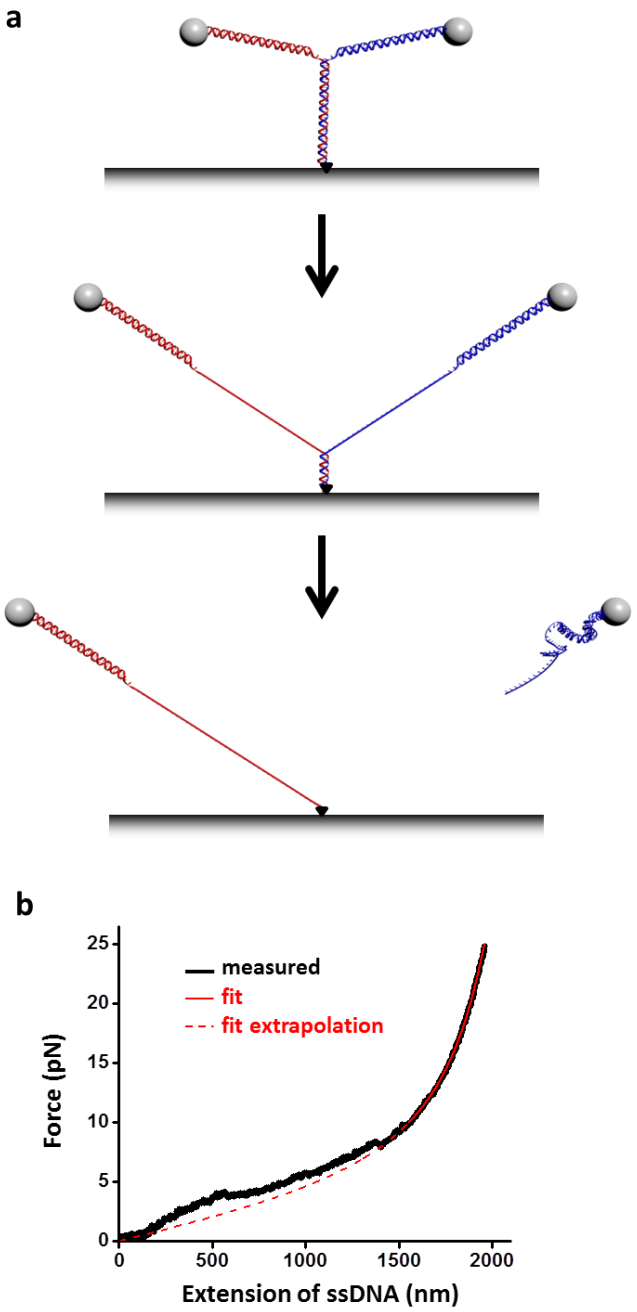

Figure S5. Generating and stretching long ssDNA tethers.

(a) Cartoons depicting the steps to generate a long ssDNA tether. The initial Y structure contained a trunk with only one strand of the trunk end attached to the coverslip surface.

The Y structure was then fully unzipped to release the other trunk strand from the surface. The remaining tether was composed of a dsDNA segment that had been one of the original arms and a newly generated long stretch of ssDNA that had been part of the original trunk dsDNA. This tether was subsequently stretched to obtain a force-extension curve of the composite dsDNA and ssDNA.

(b) Force versus extension of ssDNA. The force-extension curve of the ssDNA was obtained after removing the contribution of the dsDNA from the measured force-extension of the composite DNA. The resulting ssDNA force-extension (black) was fit to a modified freely-jointed chain model (solid red) at forces > 10 pN, yielding a persistence length of 0.765 nm, a stretch modulus of 470 pN, and a contour length of 2055 nm. Below 10 pN, an extrapolation of the fit is shown.

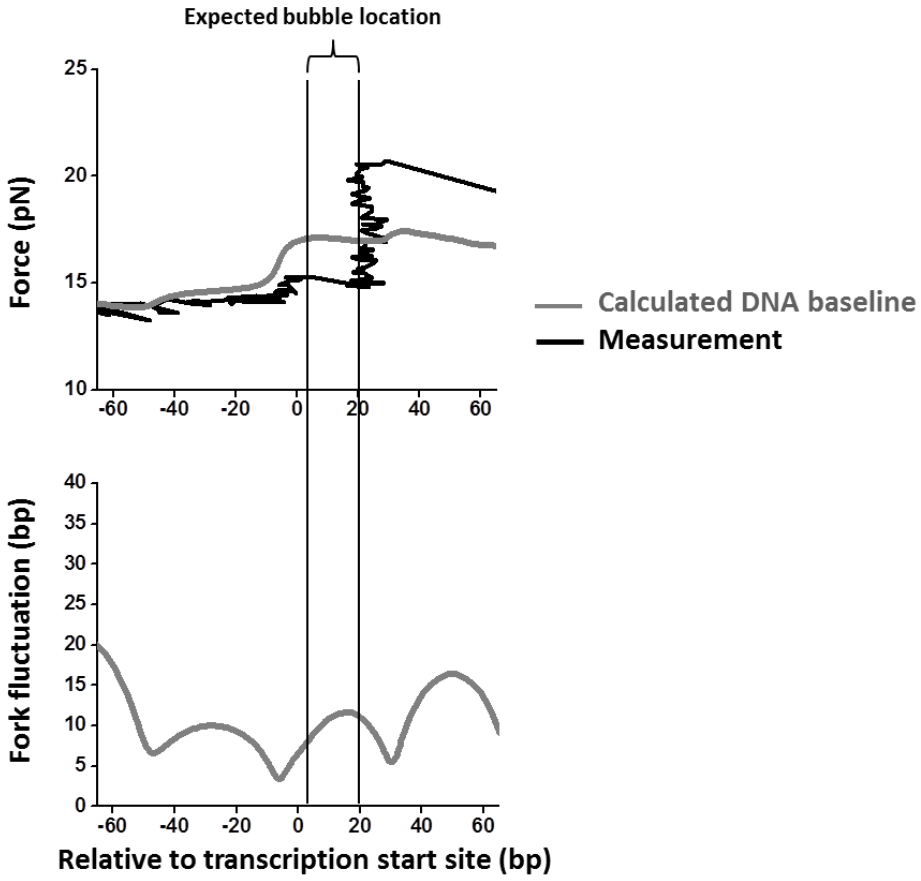

Figure S6. Fluctuations of the unzipping fork in the presence of a transcription bubble. (upper) Measured unzipping force in the presence of a paused transcription elongation complex (TEC) (black) compared with the calculated unzipping force in the absence of a TEC (grey). (lower) Calculated fork fluctuations (standard deviation of the number of base pairs unzipped) near the paused TEC. All calculations were performed for a constant trunk force of 4 pN.

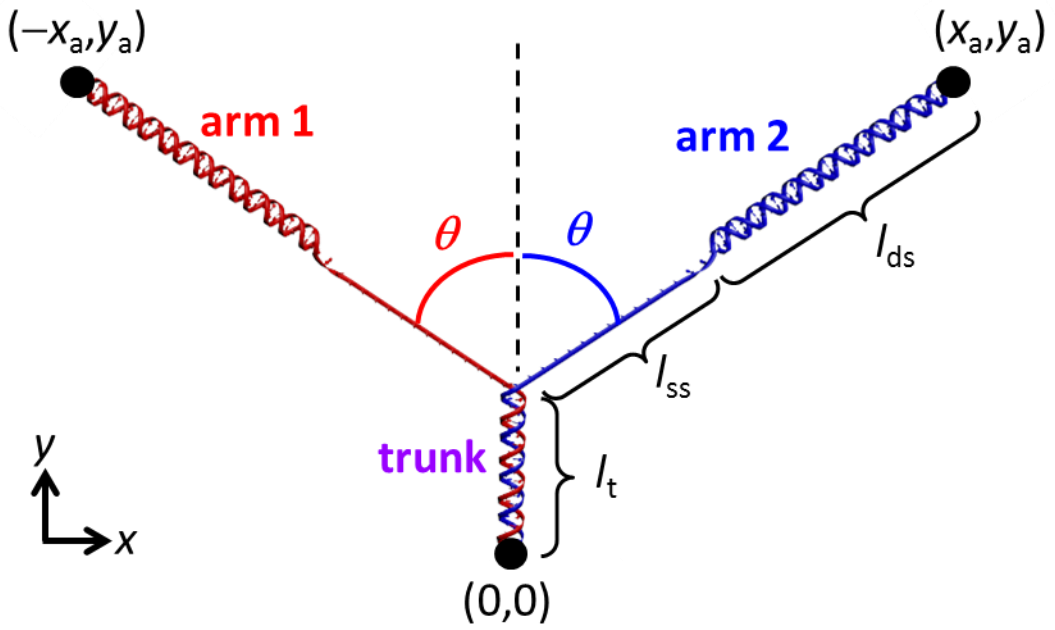

Figure S7. Geometry of the Y structure for theoretical modeling. The Y structure is confined to the *xy* plane and is symmetric about the trunk. The extension of each segment of DNA is indicated: l_t for the dsDNA trunk, l_{ss} for ssDNA in each arm, and l_{ds} for dsDNA in each arm.

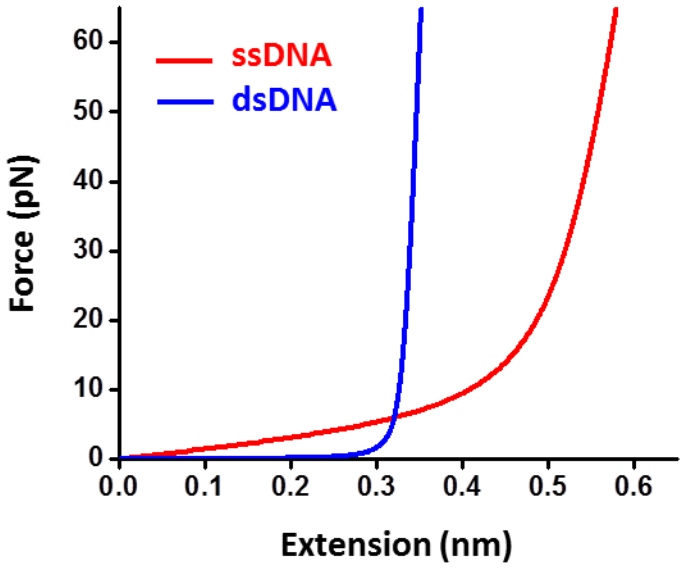

Figure S8. Force-extension curves of ssDNA and dsDNA. Shown are extensions per nucleotide of ssDNA (red) and per base pair of dsDNA (blue) as determined by measured DNA elasticity parameters. See Eqs. (1) and (2).

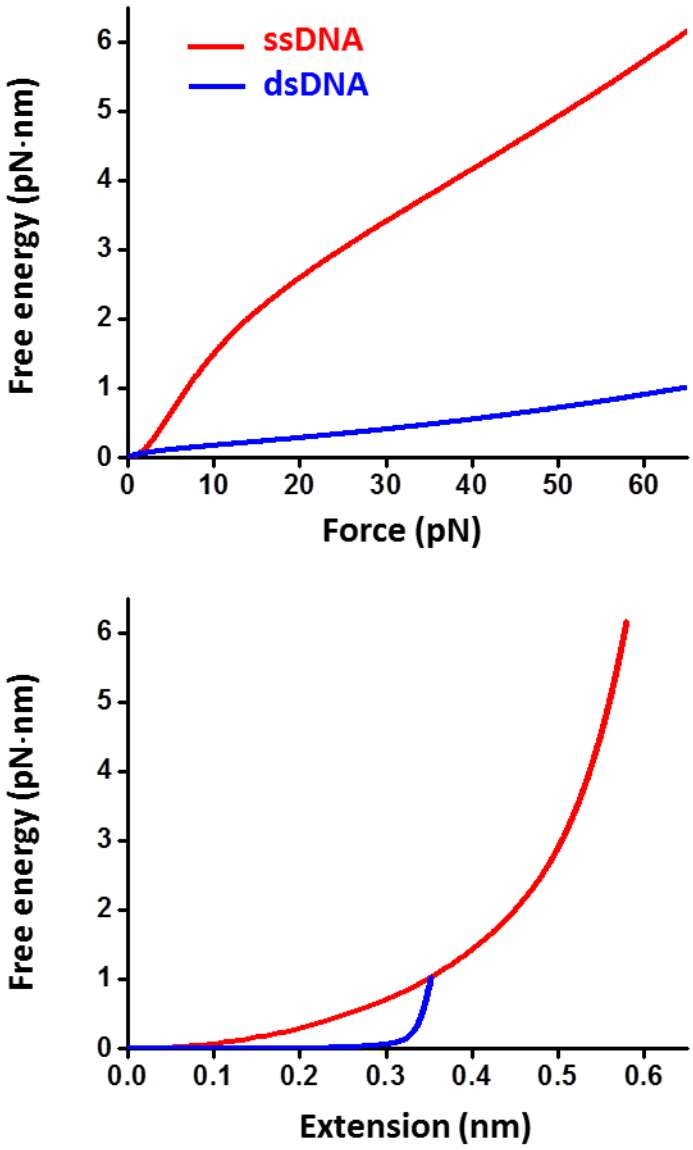

Figure S9. Energies to stretch ssDNA and dsDNA. Shown are the energies needed to stretch one nucleotide of ssDNA (red) and one base pair of dsDNA (blue) to specified extension and force.

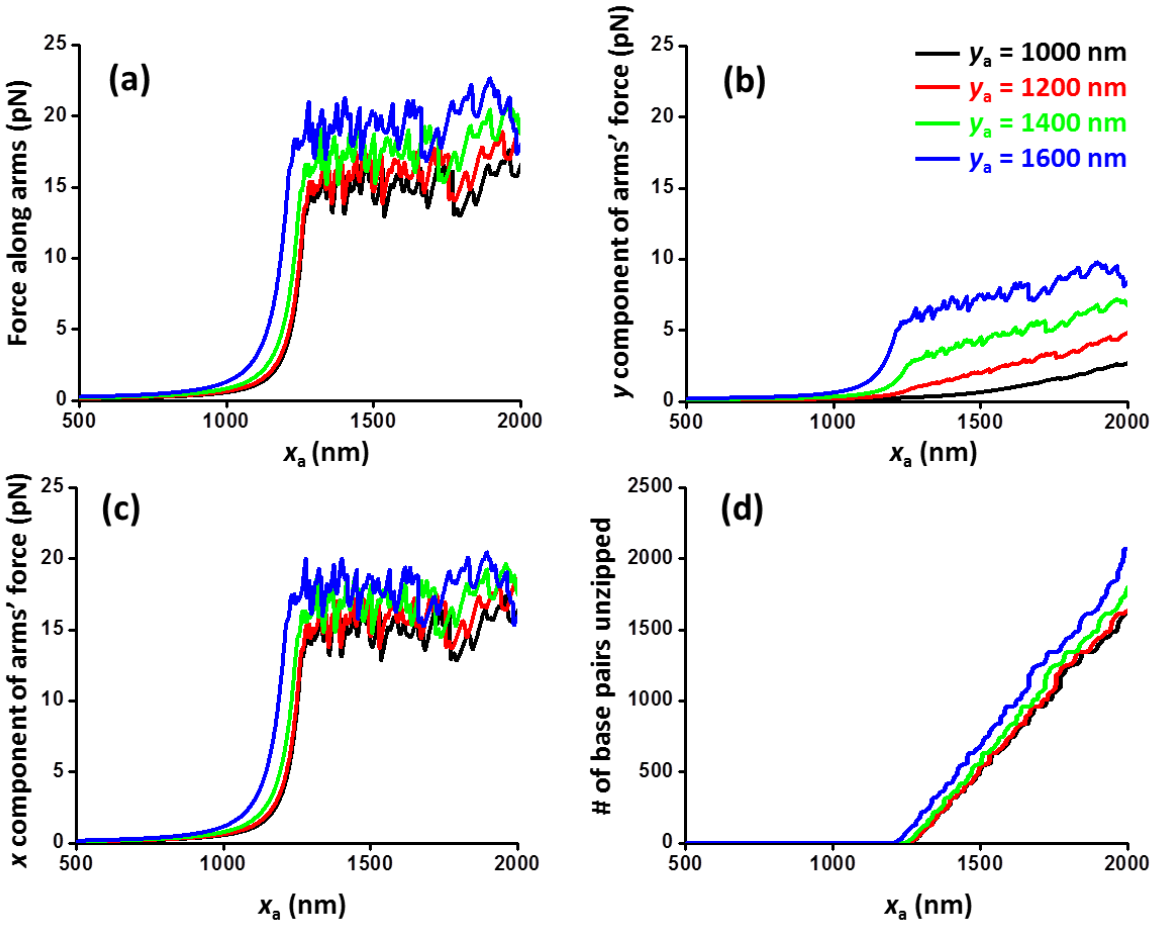

Figure S10. Forces under constant end positions of the Y structure. Results are shown for several values of y_a positions.

(a) Force along arms versus x_a.

(b) y component of arms' mean force versus x_a.

(c) x component of arms' mean force versus x_a.

(d) Number (#) of base pairs unzipped versus x_a.

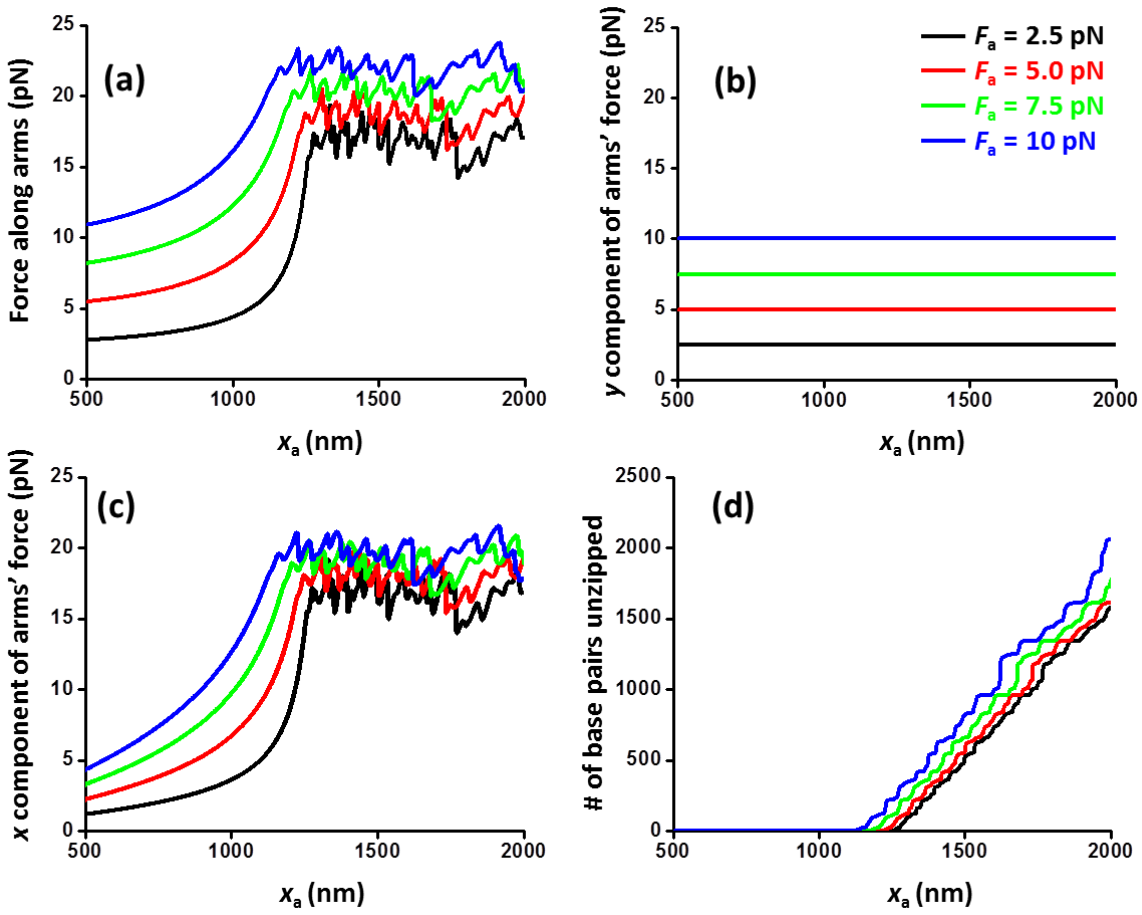

Figure S11. Arm forces under a constant trunk force of the Y structure. Results are shown for several values of the trunk forces.

(a) Force along arms versus x_{a}.

(b) y component of arms' mean force versus x_{a}.

(c) x component of arms' mean force versus x_{a}.

(d) Number (#) of base pairs unzipped versus x_{a}.

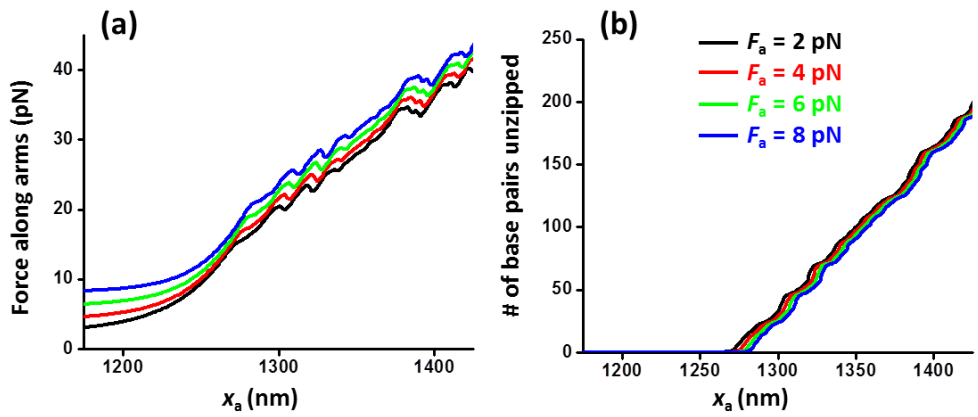

Figure S12. Arm forces under a torsionally constrained trunk of the Y structure. Results are shown for several values of the trunk forces.

(a) Force along arms versus x_{a}.

(b) Number (#) of base pairs unzipped versus x_{a}.

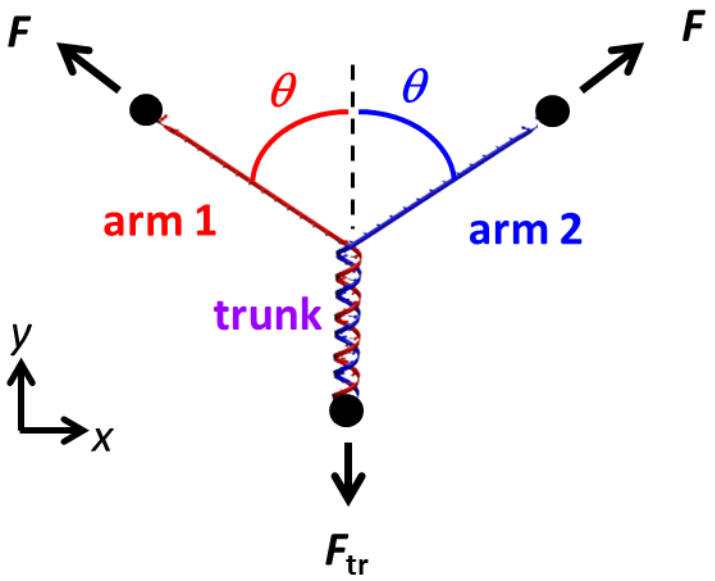

Figure S13. Geometry of the Y structure under constant forces in all three branches. The Y structure is confined to the *xy* plane and is symmetric about the trunk. Each arm consists of ssDNA held at a constant force of magnitude F at angle θ with respect to the trunk.

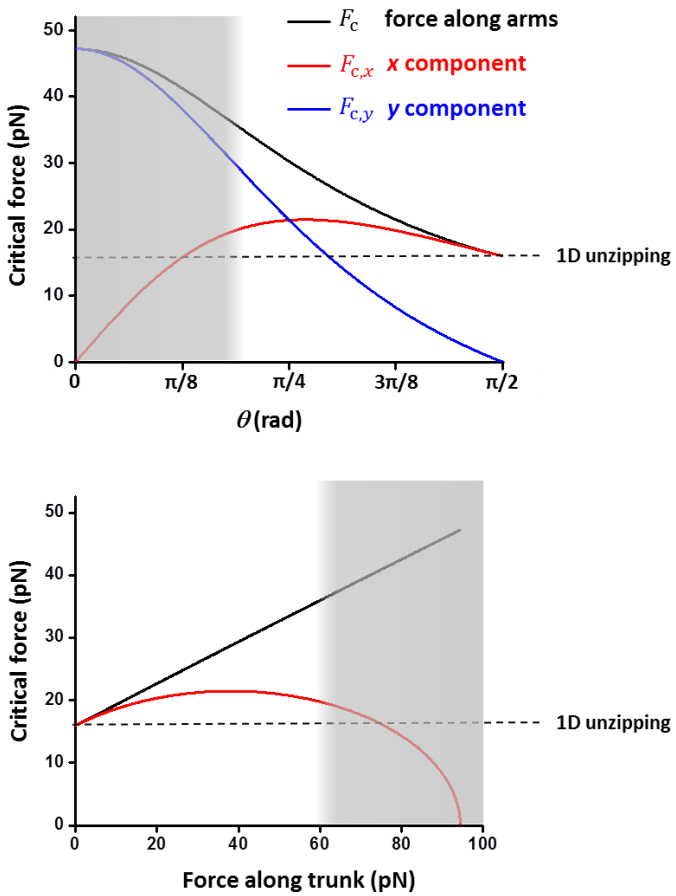

Figure S14. Critical force of the Y structure under constant force. For this calculation, the homopolymeric DNA trunk is assumed to a base pairing energy $E_{\mathrm{bp}} = 2.4\ k_{\mathrm{B}}T$. (Top panel) The critical force, at which the Y structure unzips, is plotted as a function of the angle of the applied force. $\theta = \pi/2$ corresponds to 1D unzipping where there is no force on the trunk. As trunk force increases above 65 pN, trunk DNA is expected to undergo a B-S phase transition (shaded region) which our theory does not consider. (Bottom panel) The critical force is plotted as a function of the force along the trunk for a more direct comparison with our experimental results.

Supporting Information Video 1. Simultaneous stretching, unzipping, and fluorescence.

This Y structure contained two arms of different lengths in order to make the two arms easily distinguishable, and a trunk with a paused transcription elongation complex (TEC) formed with an HA-tagged *E. coli* RNAP. The RNAP was subsequently labelled by anti-HA, which was then labeled by secondary-antibody coated quantum dots. The trunk DNA containing an RNAP was subsequently unzipped, resulting in a head-on collision of the TEC with the unzipping fork. The RNAP was found to be bound to the trunk DNA prior to encountering the unzipping fork. It was visualized by fluorescence and its precise location on the dsDNA was determined by its force signature during unzipping. After the unzipping fork passed through the bound RNAP, the RNAP was found to be retained on the template strand (the shorter Y arm). (Top) The actual images and data showing the location of the RNAP (red, fluorescence images), the trapped microspheres (green, bright field images), and the real-time measured extensions of three branches of the Y structure (white lines) as the trunk DNA was unzipped through the bound RNAP.

(Bottom) The force on the arms versus the number of base-pairs unzipping is plotted.

Supporting Information Discussion

1. Y structure construction

The Y structure DNA was constructed from three distinct dsDNA segments: two arms and the trunk (**Fig. S1**). The arms were made by restriction enzyme cuts from plasmid pMDW38 (sequence available upon request) for symmetric arms or from plasmid pRL574[1] for asymmetric arms. A single restriction cut (XhoI or SphI) in this plasmid created an overhang that was subsequently filled in with either dig-dUTP or bio-dATP by Klenow polymerase (NEB) to provide specific attachment to anti-digoxigenin or streptavidin coated microspheres respectively. A second restriction cut (BstXI or BstEII) created an overhang for ligation to an annealed trunk adapter oligos to generate a long (>30 bp) overhang on each arm. The two trunk adaptor oligos from the two arms were complementary to each other and were subsequently annealed to form Y arms with a short trunk (~30 bp). The annealed adaptor oligos were designed to create an overhang for ligation to the full length trunk. Such a design is modular so that the trunk is interchangeable. Trunk DNA was made via PCR with a primer containing a 5' fluorescein for subsequent anchoring to an anti-fluorescein surface and then cut with a restriction enzyme (AlwNI) to provide the proper overhang for ligation to the Y arms. A fluorescein and anti-fluorescein attachment has been shown to be strong (dissociation constant ~ 10^{-10} M^2) and has been previously used as a suitable single molecule linkage[3]. We found the lifetime of the fluorescein anti-fluorescein attachment to be comparable to that of digoxigenin and anti-digoxigenin attachment.

The torsionally constrained trunk was made by ligation to a torsion adapter at the end of the Y trunk. The torsional adapter was ~ 500 bp made via PCR from pMDW2 (sequence available upon request) with a 1:5 mixture of dTTP:fluorescein-dUTP to provide multiple attachment points in both strands.

For the RNAP fluorescence experiments, an 'asymmetric' Y structure was made with two arms having different lengths in order to determine to which strand RNAP remained bound after unzipping. This was accomplished by cutting the arms out of the plasmid pRL574 with restriction enzymes to create a longer DNA (dig arm with SalI and BstEII; bio arm with SapI and BstXI). For the co-directional collision template, the trunk contained a T7A1 promoter with a transcription start site located at 1065 bp from the Y-junction. For the head-on collision template, the transcription start site was located at 1108 bp from the Y-junction.

2. Quantum-dot labelled RNA polymerase

For RNA polymerase unzipping experiments, a transcription elongation complex was formed on the trunk DNA following a protocol similar to that previously established[1,4]. Briefly, the 3.7 kbp trunk DNA (10 nM) was incubated with *E. coli* RNA polymerase (100 nM) for 30 minutes at 37 °C in the transcription buffer (25 mM Tris-Cl pH 8.0, 100 mM KCl, 4 mM $MgCl_2$, 1 mM DTT, 0.4 mg/mL BSA, 7.5% glycerol, 50 μM ATP/GTP/CTP, 100 μM ApU, 1U/μL SUPERase-In). The

resulting trunk contained a transcription elongation complex paused at +20 bp from the promoter. The trunk DNA was then ligated to the short Y-arm.

The RNAP was fluorescently labeled with quantum dots using standard antibody labeling techniques which has been demonstrated not to interfere with protein-DNA binding[5]. Briefly, single molecule Y-structure tethers were formed in a microscope flow cell. Purified HA-tagged RNAP[6,7] as labeled with primary antibody to HA expressed in mouse (Covance). Excess antibodies were washed out of the chamber PBS. Quantum dots coated with secondary antibodies (Invitrogen A-10195) were flowed in to bind to the primary antibodies. Excess quantum dots were washed out of the chamber PBS.

3. Instrument design and calibration

The dual optical trapping setup was a built upon a Nikon TE200 microscope with fluorescence and bright field microscopy capabilities (**Fig. S2**). The dual trap was created from a single laser source (Spectra Physics J20, 5 W) that was split into two beams by a polarizing beam splitting cube (PBSC) into orthogonal linear polarizations. One of the polarized beams was steered by a mirror mounted on a tip-tilt piezo (MCL Nano-MTA)[8]. Although the two beams were orthogonally polarized, some interference between the two beams still existed due to the use of a high NA objective, leading to some cross talk between the two traps[9]. To minimize this, we inserted optical windows in one of the two beams so that the path length difference between the beams was set to longer than the coherence length of the laser (3 mm). The two beams

were recombined with another PBSC before entering a custom-built 'trapping port' which reflected the beams into the microscope objective with a dichroic mirror. The traps were formed at the focus of a water immersion objection (Nikon MRD07602). The two beams were collected by the condenser and split by a PBSC. Each polarized beam was detected by a quadrant photodiode (Pacific Silicon Sensor QP50-6SD2) by back focal-plane interferometry to provide positions and forces along *x* and *y* (lateral), and *z* (axial) directions for each microsphere in its trap. The flow cell was mounted on a 3D piezo stage (MCL Nano-LPQ) to allow movement of the coverglass surface relative to the traps.

Epi fluorescence was excited by a mercury arc lamp. The fluorescent cube set was designed for quantum dots with emission at 625 nm (Chroma 32214). Bright field illumination was accomplished with a red LED (625 nm, Thorlabs M625L2 and LEDD1B) which was transmitted by the 625 nm emission filter of the cube set. This allowed both the bright field and fluorescence images to be collected by the same cooled CCD (Hamamatsu ORCA-ER). To interlace the bright field and fluorescence images, the camera controller triggered the LED to turn on and off using a custom-built LED controller.

The optical traps were calibrated using previously established methods[10-12] with untethered polystyrene microspheres (489 ± 13 nm in diameter, Polysciences 09836). In brief, microsphere position calibration was carried out by scanning a surface-adhered microsphere through the trap via the 3D piezo stage to map the quadrant photodiode outputs as a function of the *x*, *y*, and *z* positions of the stage. Trap stiffness calibration was carried out using both the power

spectrum and the viscous drag methods. Briefly, for the power spectrum method, the *x*, *y*, and *z* positions of a trapped bead were measured and their power spectra were used to determine the trap stiffness along *x*, *y*, and *z* respectively. For the viscous drag method, the *x*, *y*, and *z* positions of a trapped bead were measured as the bead was moved through the solution at a constant speed along *x*, *y*, or *z* direction. The resulting viscous force versus bead displacement was then used to calculate the trap stiffness. The results from these two methods agreed within statistical uncertainty. For small displacements, the trap stiffness was determined to be 1.19 ± 0.04 pN nm^{-1} W^{-1} along *x*, 1.60 ± 0.17 pN nm^{-1} W^{-1} along *y*, and 0.31 ± 0.04 pN nm^{-1} W^{-1} along *z* for trap 1 and 1.36 ± 0.08 pN nm^{-1} W^{-1} along *x*, 1.27 ± 0.08 pN nm^{-1} W^{-1} along *y*, and 0.25 ± 0.04 pN nm^{-1} W^{-1} along *z* for trap 2, with power being that estimated for the sample plane. Maximum power used in the experiments was ~120 mW per trap at the sample plane. In all experiments on a Y structure, the microsphere displacement was limited to the linear trapping regime (< 100 nm displacement).

Although the Y-structure may lie in any plane that is formed by its surface anchor and the two trapped microspheres, in order to reduce the effect of trap center drift due to laser heating of the objective, the Y structure was extended predominately in the *xy* plane with a small *z* component (**Fig. S3**).

4. Data collection and analysis

Sample chambers were prepared using standard single molecule methods[13,14]. Briefly, a chamber was coated with anti-fluorescein (Molecular Probes) at 20 μg/mL by incubation for 10 min and then the surface was blocked with 4 mg/mL casein. Subsequently, the Y structure at 10 pM was introduced into the sample chamber and incubated for 10 min. Finally, microspheres (489 ± 13 nm, Polysciences 09836) coated with anti-digoxigenin or streptavidin were sequentially incubated in the chamber for 10 min each. During an experiment, Y structures were identified as two microspheres in close proximity to each other undergoing constrained Brownian motion. These accounted for ~10% of the total tethers in the chamber. The two microspheres were readily separated into the two traps which were placed ~ 1 μm apart and centered over the Y structure. In some cases, the two microspheres fell into the same trap. If this occurred, both microspheres were released and the process was repeated. It typically took 5-20 s to configure a Y structure for experiments.

Custom software (LabVIEW 2010) was then used to automate several routines. First, prior to trapping a Y-structure, without microspheres in the trap, baseline data were recorded as the steered trap was scanned across the *xy* (lateral) plane. These baseline data were used to make corrections to experimental data. Second, the Y-structure anchoring point to the surface was centered between the two trapped microspheres by stretching the tether with the piezo stage using an algorithm similar to that previously described[10]. Third, the height of the traps above the coverslip surface was determined by moving the coverslip towards the trapped

microspheres and detecting the *z* piezo position when the microspheres came into contact with the surface[12]. Fourth, the Y-structure was then stretched and unzipped by moving both the steered trap and the piezo stage. A constant force on the trunk during unzipping experiments was maintained by feedback on the piezo stage and laser power at 100 Hz[10].

The 3D location for the junction of the Y-structure was determined as the intersection of the lines of force from the microspheres' positions. Thus the extensions of the three branches of the Y-structure were determined from the positions of the microspheres, the Y-structure anchoring point, and the Y-structure junction location. The forces on the arms were measured directly and the force on the trunk was determined by requiring the net force at the junction to be zero. Force and extension data for each arm were used for conversion to number of base pairs unzipped[11] (see **Calculation of Y structure forces and extensions**).

During fluorescence experiments, interlaced images of bright field and fluorescence were acquired by the CCD at 31.4 frames per second. To create an overlaid image such as those shown in **Fig. 4b**, a pair of bright field and fluorescence images were pseudo-colored and combined. To overlay the Y-structure configuration to indicate the three DNA segments, the 3D Y-structure configuration as determined from the optical trapping data was projected onto the *xy* plane and displayed as three white lines for the three DNA segments. The locations of the two microspheres were used as a reference to align the Y-structure to the images.

5. Calculation of Y structure forces and extensions

During an experiment, the 3D locations and force vectors of the two trapped microspheres as well as the position of the coverslip surface were measured in real time. To fully characterize the Y structure, the force and extension of each segment of the Y structure as well as the Y structure geometry were calculated from the raw data collected by our dual trap instrument. Below is a description of this calculation.

Below we refer to the coordinate system defined in **Fig. S3**. (1) The 3D location of the Y junction was determined. The *xy* location of the Y junction was located as the intersection of the lines of *xy* forces from the microspheres' positions (**Fig. S3a**). The *z* coordinate of the junction was determined by the geometry defined by the height of the microspheres above the surface and the *y* position of the junction (**Fig. S3b**). (2) Once the position of the junction was known, the extension of each branch of the Y structure was determined as the distance between its two endpoints. (3) Finally, the force vectors on the arms were directly measured by the optical trap. The force on the trunk was determined by requiring that the net force at the junction to be zero (**Fig. S3c**). Thus, the force vector on the trunk was simply the opposite of the vector sum of the optical forces on the trapped microspheres.

The number of base pairs unzipped was calculated from the force and extension measurements described above. First, the force and extension of each branch of the Y structure were measured under lower forces (< 15 pN) prior to unzipping. These were taken as initial

characterization of the Y structure. As the Y structure was unzipped, the extension in each arm at a given force increased beyond what could be accounted for by dsDNA alone. The additional extension was attributed to ssDNA. We used the modified freely-jointed-chain model of ssDNA[10,15] to calculate the number of base pairs of ssDNA in each arm. The ssDNA in the arms was a measure of the number of base pairs unzipped.

To achieve near base pair resolution, the resulting force versus number of base pairs unzipped curve was aligned to the corresponding theoretical curve discussed in the next section using a cross-correlation method we previously developed[14,16,17] To account for minor instrumental drift, trapping-bead size variations, and DNA linker variations, the alignment allowed for a small additive shift (~ 20 bp) and a multiplicative linear stretch (~ 3%).

6. Generation and manipulation of long ssDNA

ssDNA is an important substrate, or intermediate, during replication, DNA repair and recombination, where long stretches of thousands of base pairs of ssDNA are operated on by a variety of proteins. It has been experimentally challenging to generate and manipulate long ssDNA of arbitrary sequence using an optical trap. Previous methods relying on DNA stretching require the application of high force (~ 65 pN) and/or chemical reagents[15,18,19] or the use of enzymatic reactions[20] to facilitate strand separation. Methods using DNA unzipping do not subject a DNA molecule to excessive forces but yield ssDNA of complementary sequences that anneal upon force reduction[11,21].

Here, we demonstrate the use of the Y structure, first to generate ssDNA of many kilo-base pairs of arbitrary sequence, and then to manipulate it from low to high forces. In order to generate ssDNA, we used a Y-structure version with only one strand of its trunk end attached to the microscope coverslip (**Fig. 1a**). The dsDNA trunk was then unzipped to completion using a method similar to that described in **Fig. 1** and **Fig. 2**. Once the trunk was fully unzipped, one strand of the trunk remained attached to the coverslip and was composed of one dsDNA arm and the ssDNA of the trunk of the original Y structure (**Fig. S5a**). The other strand, and its associated arm, retracted to their trapped microsphere which was subsequently released into solution. The remaining tether was then stretched with one of the traps and its force-extension curve was measured. After removing the contribution to the force-extension from the dsDNA arm[10], the force-extension curve of the ssDNA was obtained (**Fig. S5b**). The force-extension of ssDNA was well characterized by a modified freely-jointed chain model[15] at forces > 10 pN, yielding fit parameters in good agreement with those previously established[11,15]. Below this force, the relation showed less well defined features, as a result of the formation of secondary structures in the ssDNA at low forces[22,23].

7. Mapping the TEC structure

We found that when DNA containing a TEC was unzipped co-directionally with the direction of transcription, a force drop occurred a few base pairs before the expected location of the edge of the transcription bubble. We interpret this as a result of thermal fluctuations of the

unzipping fork. As DNA is unzipped, the unzipping fork is expected to fluctuate among multiple energy states, at rates much faster than the unzipping speed. Therefore, the measured fork position represents the mean value for the fork position[21,24]. The extent of fluctuations is DNA sequence-dependent but is of the order of 5-10 base pairs (**Fig. S6**). As the fork approaches a DNA bubble, the fork's excursions away from the mean may encounter the DNA bubble. At this point, the fork will immediately open the entire bubble and become trapped in the much lower energy open state. Thus, the location of the start of a bubble will always be detected closer to the unzipping fork than the bubble's actual edge. The extent of the shift will be related to the local DNA sequence, the temperature, and the rate of unzipping. By contrast, the location of the end of the bubble can be determined with much more certainty. Therefore, when the region of force drop is used to determine the bubble size, the size is always over-estimated.

8. Theoretical models of Y structure unzipping

We have extended a previous theoretical model of 1D DNA unzipping using equilibrium statistical mechanics methods[21,25-27] to model 2D DNA unzipping of a Y structure.

For this section, to simplify notation, we consider a symmetric Y structure initially consisting of two arms, each of n_{arm} base pairs of dsDNA, and a trunk of n_{tr} base pairs of dsDNA (**Fig. S7**). As the trunk is unzipped by n base pairs, n nucleotides of ssDNA are added to each arm while the trunk reduces to $n_{\mathrm{tr}} - n$ base pairs of dsDNA. For simplicity, we assume that the trunk is

unzipped by two arm forces symmetric about the trunk, and the Y structure lies in the xy plane with the trunk end at $0,0$, arm 1 end at $-x_{\mathrm{a}}, y_{\mathrm{a}}$, and arm 2 end at $+x_{\mathrm{a}}, y_{\mathrm{a}}$. The junction location and forces in each branch are determined by requiring the net force at the junction to be zero, using the measured force-extension relations.

The force-extension relation per nucleotide of ssDNA[15] is:

$$\frac{s_{\mathrm{ss}}}{L_{0\_\mathrm{ss}}} = \coth\left(\frac{2f_{\mathrm{ss}}L_{\mathrm{p\_ss}}}{k_{\mathrm{B}}T}\right) - \frac{k_{\mathrm{B}}T}{2f_{\mathrm{ss}}L_{\mathrm{p\_ss}}}\left(1+\frac{f_{\mathrm{ss}}}{K_{0\_\mathrm{ss}}}\right), \quad (1)$$

where f_{ss} is the force, s_{ss} the extension per nucleotide, L_{0_ss} the contour length per nucleotide of ssDNA, $L_{\mathrm{p\_ss}}$ the persistence length of ssDNA, K_{0_ss} the stretch modulus of ssDNA, and $k_{\mathrm{B}}T$ the thermal energy. Using the Y structure as described in the main text (**Fig. S5b**), we measured L_{0_ss}, $L_{\mathrm{p\_ss}}$, K_{0_ss}, and $k_{\mathrm{B}}T$ to be 0.55 nm, 0.79 nm, 470 pN, and 4.11 pN·nm respectively under our experimental conditions (**Fig. S8**).

The force-extension per base pair of dsDNA[10] is:

$$f_{\mathrm{ds}} = \frac{k_{\mathrm{B}}T}{L_{\mathrm{p\_ds}}}\left(\frac{1}{4\left(1-s_{\mathrm{ds}}/L_{0\_\mathrm{ds}}+f_{\mathrm{ds}}/K_{0\_\mathrm{ds}}\right)^2}-\frac{1}{4}+\frac{s_{\mathrm{ds}}}{L_{0\_\mathrm{ds}}}-\frac{f_{\mathrm{ds}}}{K_{0\_\mathrm{ds}}}\right), \quad (2)$$

where f_{ds} is the force, s the extension per base pair, L_{0_ds} the contour length per base pair of dsDNA, $L_{\mathrm{p\_ds}}$ the persistence length of dsDNA, and K_{0_ds} the stretch modulus of dsDNA. We used previously measured values of L_{0_ds}, $L_{\mathrm{p\_ds}}$, and K_{0_ds} of 0.34 nm, 43 nm, and 1200 pN respectively[10] (**Fig. S8**).

Once x_{a}, y_{a}, and n are specified and the ssDNA and dsDNA elastic properties are determined, the junction location is determined based on force balance, yielding the trunk extension l_{t}, ssDNA extension in each arm l_{ss}, and dsDNA extension in each arm l_{ds}, as well as forces in each branch (**Fig. S7**). Thus the state of the Y structure is fully defined by the positions of the three end points of the Y structure and the number of base pairs unzipped, i.e., x_{a}, y_{a}, and n. Below we consider unzipping under four different scenarios.

The Y structure under constant end positions

Consider a scenario where the trunk DNA of the Y structure is unzipped such that the ends of the arms are at specified positions (i.e., x_{a} and y_{a} are given and held fixed). Under thermal agitation, the fork junction may still fluctuate over multiple states, each with a different number of base pairs (n) unzipped. We wish to find the equilibrium fork junction position and the equilibrium forces in the three branches. Our general strategy is to determine the free energies at all possible states, use these energies to define the partition function of the system, and then use the partition function to determine the equilibrium value (mean value) of any parameter of interest.

The free energy of the Y structure at a given state consists of two distinct components:

$$G\ n; x_{\mathrm{a}}, y_{\mathrm{a}}\ = G_{DNA}\ n\ + G_{\mathrm{stretch}}\ n; x_{\mathrm{a}}, y_{\mathrm{a}}\ \ . \tag{3}$$

The first term $G_{DNA}(n)$ is free energy increase due to the loss of base pairing of the first n base pairs unzipped, and can be determined using the nearest-neighbor model with corrections that

take into account the temperature and salt conditions used in the experiments[26]. The second term $G_{\mathrm{stretch}}\ n; x_{\mathrm{a}}, y_{\mathrm{a}}$ is the work to stretch each branch of the Y structure to the specified state:

$$G_{\mathrm{stretch}}\ n; x_{\mathrm{a}}, y_{\mathrm{a}}\ = 2G_{\mathrm{ds,arm}}\ n_{\mathrm{arm}}, l_{\mathrm{ds}}\ + 2G_{\mathrm{ss,arm}}\ n, l_{\mathrm{ss}}\ +\ G_{\mathrm{ds,trunk}}\ n_{\mathrm{tr}} - n, l_{\mathrm{t}}\ , \tag{4}$$

For ssDNA of n nucleotides to stretch to extension l (**Fig. S9**), the free energy is

$$G_{\mathrm{ss}}\ n, l\ = n\ \int_0^{l/n} f_{\mathrm{ss}}\ s_{\mathrm{ss}}\ \ ds_{\mathrm{ss}}\ . \tag{5}$$

For dsDNA of n base pairs to stretch to extension l (**Fig. S9**), the free energy is

$$G_{\mathrm{ds}}\ n, l\ = n\ \int_0^{l/n} f_{\mathrm{ds}}\ s_{\mathrm{ds}}\ \ ds_{\mathrm{ds}}. \tag{6}$$

Given x_{a} and y_{a}, we numerically calculate the extensions of all DNA segments for each possible value of n using the "fsolve" routine of the SciPy package of Python. The results of this calculation are then used to calculate $G\ n; x_{\mathrm{a}}, y_{\mathrm{a}}$, which yields the partition function. The average number of base pairs unzipped n and the average force F_i (i = 1 to 3, one for each branch) are determined from the partition function:

$$n\ = \frac{\sum_n n\ exp\ -G\ n; x_{\mathrm{a}}, y_{\mathrm{a}}\ \ k_{\mathrm{B}}T}{\sum_n exp\ -G\ n; x_{\mathrm{a}}, y_{\mathrm{a}}\ \ k_{\mathrm{B}}T} \tag{7}$$

$$F_i\ = \frac{\sum_n F_i\ exp\ -G\ n; x_{\mathrm{a}}, y_{\mathrm{a}}\ \ k_{\mathrm{B}}T}{\sum_n exp\ -G\ n; x_{\mathrm{a}}, y_{\mathrm{a}}\ \ k_{\mathrm{B}}T} \tag{8}$$

Fig. S10 shows some results of these calculations. At a small value of $y_{\mathrm{a}} - l_{\mathrm{t}}$, the mean unzipping force along arms is comparable to the corresponding 1D unzipping force which

fluctuates around ~ 15 pN. The force along arms and the trunk force increase with a more extended Y structure in y and/or more base pairs unzipped.

The Y structure under constant trunk force

Next we consider a scenario where the trunk DNA of the Y structure is unzipped under a constant trunk force ($F_{\mathrm{tr}} = 2F_{\mathrm{a},y}$) such that the x coordinates of the ends of the arms are specified (i.e., F_{tr} and x_{a} are given and held fixed). To calculate arm force in this situation, the free energy must be a function of x_{a} and F_{tr} instead of x_{a} and y_{a}. We refer to this free energy as $G_1\ n; x_{\mathrm{a}}, F_{\mathrm{tr}}$ which relates to $G\ n; x_{\mathrm{a}}, y_{\mathrm{a}}$ via the Legendre transform by subtracting the product of the conjugate variables y_{a} and F_{tr}:

$$G_1\ n; x_{\mathrm{a}}, F_{\mathrm{tr}} = G\ n; x_{\mathrm{a}}, y_{\mathrm{a}} - y_{\mathrm{a}} F_{\mathrm{tr}}. \quad (9)$$

Since

$$\frac{\partial G\ n; x_{\mathrm{a}}, y_{\mathrm{a}}}{\partial y_{\mathrm{a}}} = F_{\mathrm{tr}}, \quad (10)$$

Eq. (10) allows Eq. (9) to be expressed solely in terms of n, x_{a}, and F_{tr}. Eq. (9) indicates that the free energy $G_1\ n; x_{\mathrm{a}}, F_{\mathrm{tr}}$ lowers with an increase in the trunk force.

Once $G_1\ n; x_{\mathrm{a}}, F_{\mathrm{tr}}$ is determined, the arm force and the number of base pairs unzipped can be found using a partition function of the form in Eqs. (7) and (8) by replacing $G\ n; x_{\mathrm{a}}, y_{\mathrm{a}}$ with $G_1\ n; x_{\mathrm{a}}, F_{\mathrm{tr}}$. **Fig. S11** shows some results of these calculations. As with the scenario where the ends of the Y structure are held at fixed positions, this scenario also shows that at low trunk

force, the arm force is comparable to the 1D unzipping force. As the trunk force increases, the arm force also increases.

The Y structure under torsional constraint

We now consider a scenario where the trunk end is torsionally constrained and the trunk DNA is unzipped under a constant trunk force ($F_{\mathrm{tr}} = 2F_{\mathrm{a},y}$) such that the x coordinates of the ends of the arms are specified (i.e., F_{tr} and x_{a} are given and held fixed). As the trunk DNA is unzipped, the linking number in the trunk remains constant while the trunk shortens, resulting in overtwisting of the trunk. Continued torque buildup will eventually lead to a phase transition to plectonemic DNA or P-DNA[28-32]. We will limit our discussion to consider only the B-DNA regime prior to any phase transition.

To calculate the arm force, the free energy outlined in the previous section needs to be modified to take into account the torsional energy in the trunk. Torsional energy may be expressed in terms of the degree of supercoiling, σ, defined as the number of turns introduced into the DNA per natural number of turns in the DNA. Under moderate forces and small degrees of supercoiling, the twist energy depends on σ quadratically and is also a function of the force (F) in the DNA[31,33]:

$$G_{\mathrm{twist}}\ F, \sigma, L_0\ = + \frac{L_0 c_s}{2} \sigma^2, \tag{11}$$

with

$$c_s = k_{\mathrm{B}}TC\omega_0^2 \left(1 - \frac{C}{4L_{\mathrm{p\_ds}}} \left(\frac{k_{\mathrm{B}}T}{L_{\mathrm{p\_ds}}F}\right)^{1/2}\right), \quad (12)$$

where $\omega_0 = 2\pi/(3.6\ \mathrm{nm})$ is the conversion between natural angle of rotation and contour length, $C = 100$ nm the intrinsic twist persistence length[31], and L_0 contour length of the dsDNA. This expression is valid until the onset of a phase transition from B-DNA to another phase. The force dependence of c_s also implies that twist influences DNA extension. The force-extension relation of the dsDNA shown in Eq. (2) needs to be slightly revised[31,33] to consider contribution from twist.

For the torsionally constrained trunk in the Y structure, σ and L_0 are directly coupled via the number of base pairs unzipped n: $\sigma = \frac{n}{n_{\mathrm{tr}}-n}$, and $L_0 = (n_{\mathrm{tr}} - n)\, L_{0\_\mathrm{ds}}$. Therefore,

$$G_{\mathrm{twist}}(F_{\mathrm{tr}}, \sigma, L_0) = G_{\mathrm{twist}}(F_{\mathrm{tr}}, n)\ . \quad (13)$$

The free energy of the Y structure after taking into consideration the torsion in the trunk is:

$$G_2(n; x_{\mathrm{a}}, F_{\mathrm{tr}}) = G_1(n; x_{\mathrm{a}}, F_{\mathrm{tr}}) + G_{\mathrm{twist}}(F_{\mathrm{tr}}, n)\ . \quad (14)$$

This additional torsional energy term is very significant as it predicts a steep increase in torsional energy even when a small number of base pairs are unzipped. In addition, to remain in the region of B-DNA, σ must be small (< 0.04 at 2 pN of trunk force) after which the existence of plectonemes must be considered[29]. This puts a limit on the number of base pairs that can be unzipped before plectonemes begin to form in the trunk DNA. For a 4 kb trunk, this is only about ~ 160 bp.

Once $G_2\ n; x_{\mathrm{a}}, F_{\mathrm{tr}}$ is determined, the arm force and the number of base pairs unzipped can be found using a partition function of the form in Eqs. (7) and (8) by replacing $G\ n; x_{\mathrm{a}}, y_{\mathrm{a}}$ with $G_2\ n; x_{\mathrm{a}}, F_{\mathrm{tr}}$. As shown in **Fig. S12**, the force required to unzip torsionally constrained trunk DNA significantly differs from that for unzipping torsionally relaxed trunk DNA (**Fig. S11**). The steep force rise is a strong signature of torsional constraint and is readily identifiable in single molecule experiments.

The Y structure under constant forces

To gain an intuitive understanding of the unzipping force for the Y structure, we consider unzipping of a homopolymeric Y structure under constant forces in all three branches. For simplicity, we consider a symmetric Y structure initially consisting of no dsDNA arms (i.e., $n_{\mathrm{arm}} = 0$) and a trunk of n_{tr} base pairs of dsDNA (**Fig. S13**). The force in each arm is held constant with a magnitude F at an angle θ with respect to the y axis. The trunk force is thus also held constant with a magnitude $F_{\mathrm{tr}} = 2F\cos\theta$. For a homopolymeric DNA trunk, each base has the same magnitude of base pairing energy (E_{bp}). The free energy of the system is thus composed of the free energy increase due to the loss of base pairing of the first n base pairs unzipped and the DNA stretching energy in all three branches under constant forces:

$$G_3\ n; F, \theta\ = n\,E_{\mathrm{bp}} - 2n \int_0^F s_{\mathrm{ss}}\ F'\ dF'\ - (n_{\mathrm{tr}} - n) \int_0^{2F\cos\theta} s_{\mathrm{ds}}\ F'\ dF'\ . \qquad (15)$$

We will eliminate the term that does not depend on n because this term does not contribute to partitioning of the states:

$$\Delta G_3\ n;F,\theta\ = n\,E_{\mathrm{bp}} - 2n\int_0^F s_{\mathrm{ss}}\ F'\ dF' + n\int_0^{2F\cos\theta} s_{\mathrm{ds}}\ F'\ dF'$$

$$= n\ E_{\mathrm{bp}} - 2\int_0^F s_{\mathrm{ss}}\ F'\ dF' + \int_0^{2F\cos\theta} s_{\mathrm{ds}}\ F'\ dF'\ . \qquad (16)$$

Therefore, the presence of a trunk force term (the last term) which has the same sign as the base-pairing energy indicates stabilization of the trunk relative to the 1D unzipping case.

When $\theta = \frac{\pi}{2}$, this corresponds to 1D unzipping which has been shown to have a critical transition from DNA being fully base paired to fully unzipped as force in increased above a critical value[34,35]. Therefore, we expect a similar transition to occur for unzipping of the Y structure. Indeed, since $\Delta G_3\ n;F,\theta\ $ is proportional to n, the minimum free energy state corresponds to either $n = 0$ (trunk DNA remains fully double stranded) when $F < F_{\mathrm{c}}$ or $n = n_{\mathrm{tr}}$ (trunk is fully unzipped) when $F > F_{\mathrm{c}}$. At the critical force $F = F_{\mathrm{c}}$, $\Delta G_3\ n;F,\theta\ $ is independent of n and thus the fork fluctuates between these extremes. As shown in **Fig. S14**, the calculation is valid for trunk forces < 65 pN, at which the trunk undergoes a B-S transition[36,37]. As θ increases towards $\theta = \frac{\pi}{2}$ (1D unzipping limit), F_{c} decreases while its *z* component $F_{\mathrm{c},z}$ decreases more steeply. Consequently, F_{c} increases with an increase in $F_{\mathrm{c,tr}} = 2F_{\mathrm{c},z}$. $F_{\mathrm{c},x}$, the *x* component F_{c}, is greater than the 1D unzipping force over the valid range of the theory.

We will specifically evaluate how F_{c} and $F_{\mathrm{c},x}$ vary with θ as θ decrease from $\theta = \pi/2$ (1D unzipping). The first derivative of $F_{\mathrm{c}}(\theta)$ with respect to θ is:

$$\frac{dF_c}{d\theta} = \frac{\partial \Delta G_3}{\partial \theta} \frac{\partial \Delta G_3}{\partial F_c} = \frac{2F_c \sin\theta s_{ds} \; 2F_c \cos\theta}{-2s_{ss} \; F_c + 2\cos\theta s_{ds} \; 2F_c \cos\theta}. \quad (17)$$

This gives $\frac{dF_c}{d\theta}_{\theta=\pi/2} = 0$. The second derivative of $F_c(\theta)$ with respect to θ at $\theta = \frac{\pi}{2}$ is:

$$\frac{d^2F_c}{d\theta^2}_{\theta=\pi/2} = \frac{2{F_c}^2}{s_{ss} \; F_c} \frac{ds_{ds}}{dF}_{F=0} > 0. \quad (18)$$

Since $\frac{d^2F_c}{d\theta^2}_{\theta=\pi/2}$ is always positive, F_c must increase as force is applied to the trunk. Next we examine the x component of the force $F_{c,x}$.

$$\frac{dF_{c,x}}{d\theta}_{\theta=\pi/2} = 0 \quad (19)$$

$$\frac{d^2F_{c,x}}{d\theta^2}_{\theta=\pi/2} = \frac{d^2F_c}{d\theta^2}_{\theta=\pi/2} - F_c = \frac{2{F_c}^2}{s_{ss} \; F_c} \frac{ds_{ds}}{dF}_{F=0} - F_c \quad (20)$$

Since $\frac{dF}{ds_{ds}}_{F=0} < \frac{2F_c}{s_{ss} \; F_c}$ because dsDNA has a low stiffness under a small force, $\frac{d^2F_{c,x}}{d\theta^2}_{\theta=\pi/2} > 0$.

Therefore, $F_{c,x}$ will also increase as the trunk is extended.

References

1) Schafer, D. A., Gelles, J., Sheetz, M. P. & Landick, R. Transcription by single molecules of RNA polymerase observed by light microscopy. ***Nature*** 352, 444-448 (1991).

2) Omelyanenko, V. G., Jiskoot, W. & Herron, J. N. Role of electrostatic interactions in the binding of fluorescein by anti-fluorescein antibody 4-4-20. ***Biochemistry*** 32, 10423-10429 (1993).

3) Bryant, Z., Stone, M. D., Gore, J., Smith, S. B., Cozzarelli, N. R. & Bustamante, C. Structural transitions and elasticity from torque measurements on DNA. ***Nature*** 424, 338-341 (2003).

4) Yin, H., Wang, M. D., Svoboda, K., Landick, R., Block, S. M. & Gelles, J. Transcription against an applied force. ***Science*** 270, 1653-1657 (1995).

5) Wang, H., Tessmer, I., Croteau, D. L., Erie, D. A. & Van Houten, B. Functional characterization and atomic force microscopy of a DNA repair protein conjugated to a quantum dot. ***Nano Lett*** 8, 1631-1637 (2008).

6) Bai, L., Fulbright, R. M. & Wang, M. D. Mechanochemical kinetics of transcription elongation. ***Phys Rev Lett*** 98, 068103 (2007).

7) Jin, J., Bai, L., Johnson, D. S., Fulbright, R. M., Kireeva, M. L., Kashlev, M. & Wang, M. D. Synergistic action of RNA polymerases in overcoming the nucleosomal barrier. ***Nat Struct Mol Biol*** 17, 745-752 (2010).

8) Moffitt, J. R., Chemla, Y. R., Izhaky, D. & Bustamante, C. Differential detection of dual traps improves the spatial resolution of optical tweezers. ***Proc Natl Acad Sci U S A*** 103, 9006-9011 (2006).

9) Mangeol, P. & Bockelmann, U. Interference and crosstalk in double optical tweezers using a single laser source. ***Rev Sci Instrum*** 79 (2008).

10) Wang, M. D., Yin, H., Landick, R., Gelles, J. & Block, S. M. Stretching DNA with optical tweezers. ***Biophys J*** 72, 1335-1346 (1997).

11) Koch, S. J., Shundrovsky, A., Jantzen, B. C. & Wang, M. D. Probing protein-DNA interactions by unzipping a single DNA double helix. ***Biophys J*** 83, 1098-1105 (2002).

12) Deufel, C. & Wang, M. D. Detection of forces and displacements along the axial direction in an optical trap. ***Biophys J*** 90, 657-667 (2006).

13) Brower-Toland, B. & Wang, M. D. Use of optical trapping techniques to study single-nucleosome dynamics. ***Methods Enzymol*** 376, 62-72 (2004).

14) Li, M. & Wang, M. D. Unzipping single DNA molecules to study nucleosome structure and dynamics. ***Methods Enzymol*** 513, 29-58 (2012).

15) Smith, S. B., Cui, Y. & Bustamante, C. Overstretching B-DNA: the elastic response of individual double-stranded and single-stranded DNA molecules. ***Science*** 271, 795-799 (1996).

16) Shundrovsky, A., Smith, C. L., Lis, J. T., Peterson, C. L. & Wang, M. D. Probing SWI/SNF remodeling of the nucleosome by unzipping single DNA molecules. ***Nat Struct Mol Biol*** 13, 549-554 (2006).

17) Hall, M. A., Shundrovsky, A., Bai, L., Fulbright, R. M., Lis, J. T. & Wang, M. D. High-resolution dynamic mapping of histone-DNA interactions in a nucleosome. ***Nat Struct Mol Biol*** 16, 124-129 (2009).

18) Hegner, M., Smith, S. B. & Bustamante, C. Polymerization and mechanical properties of single RecA-DNA filaments. ***Proc Natl Acad Sci U S A*** 96, 10109-10114 (1999).

19) Candelli, A., Hoekstra, T. P., Farge, G., Gross, P., Peterman, E. J. & Wuite, G. J. A toolbox for generating single-stranded DNA in optical tweezers experiments. ***Biopolymers*** 99, 611-620 (2013).

20) Ibarra, B., Chemla, Y. R., Plyasunov, S., Smith, S. B., Lazaro, J. M., Salas, M. & Bustamante, C. Proofreading dynamics of a processive DNA polymerase. ***EMBO J*** 28, 2794-2802 (2009).

21) Bockelmann, U., EssevazRoulet, B. & Heslot, F. Molecular stick-slip motion revealed by opening DNA with piconewton forces. ***Phys Rev Lett*** 79, 4489-4492 (1997).

22) Dessinges, M. N., Maier, B., Zhang, Y., Peliti, M., Bensimon, D. & Croquette, V. Stretching single stranded DNA, a model polyelectrolyte. ***Phys Rev Lett*** 89, 248102 (2002).

23) Johnson, D. S., Bai, L., Smith, B. Y., Patel, S. S. & Wang, M. D. Single-molecule studies reveal dynamics of DNA unwinding by the ring-shaped T7 helicase. ***Cell*** 129, 1299-1309 (2007).

24) Bockelmann, U., Essevaz-Roulet, B. & Heslot, F. DNA strand separation studied by single molecule force measurements. ***Phys Rev E*** 58, 2386-2394 (1998).

25) Bockelmann, U., Thomen, P., Essevaz-Roulet, B., Viasnoff, V. & Heslot, F. Unzipping DNA with optical tweezers: high sequence sensitivity and force flips. ***Biophys J*** 82, 1537-1553 (2002).

26) Huguet, J. M., Bizarro, C. V., Forns, N., Smith, S. B., Bustamante, C. & Ritort, F. Single-molecule derivation of salt dependent base-pair free energies in DNA. ***Proc Natl Acad Sci U S A*** 107, 15431-15436 (2010).

27) Gross, P., Laurens, N., Oddershede, L. B., Bockelmann, U., Peterman, E. J. G. & Wuite, G. J. L. Quantifying how DNA stretches, melts and changes twist under tension. ***Nat Phys*** 7, 731-736 (2011).

28) Deufel, C., Forth, S., Simmons, C. R., Dejgosha, S. & Wang, M. D. Nanofabricated quartz cylinders for angular trapping: DNA supercoiling torque detection. ***Nat Methods*** 4, 223-225 (2007).

29) Forth, S., Deufel, C., Sheinin, M. Y., Daniels, B., Sethna, J. P. & Wang, M. D. Abrupt buckling transition observed during the plectoneme formation of individual DNA molecules. ***Phys Rev Lett*** 100, 148301 (2008).

30) Daniels, B. C., Forth, S., Sheinin, M. Y., Wang, M. D. & Sethna, J. P. Discontinuities at the DNA supercoiling transition. ***Phys Rev E Stat Nonlin Soft Matter Phys*** 80, 040901 (2009).

31) Sheinin, M. Y. & Wang, M. D. Twist-stretch coupling and phase transition during DNA supercoiling. ***Phys Chem Chem Phys*** 11, 4800-4803 (2009).

32) Forth, S., Sheinin, M. Y., Inman, J. & Wang, M. D. Torque measurement at the single-molecule level. ***Annu Rev Biophys*** 42, 583-604 (2013).

33) Marko, J. F. Torque and dynamics of linking number relaxation in stretched supercoiled DNA. ***Phys Rev E Stat Nonlin Soft Matter Phys*** 76, 021926 (2007).

34) Lubensky, D. K. & Nelson, D. R. Single molecule statistics and the polynucleotide unzipping transition. ***Phys Rev E Stat Nonlin Soft Matter Phys*** 65, 031917 (2002).

35) Danilowicz, C., Coljee, V. W., Bouzigues, C., Lubensky, D. K., Nelson, D. R. & Prentiss, M. DNA unzipped under a constant force exhibits multiple metastable intermediates. ***Proc Natl Acad Sci U S A*** 100, 1694-1699 (2003).

36) King, G. A., Gross, P., Bockelmann, U., Modesti, M., Wuite, G. J. & Peterman, E. J. Revealing the competition between peeled ssDNA, melting bubbles, and S-DNA during DNA overstretching using fluorescence microscopy. ***Proc Natl Acad Sci U S A*** 110, 3859-3864 (2013).

37) Zhang, X., Chen, H., Le, S., Rouzina, I., Doyle, P. S. & Yan, J. Revealing the competition between peeled ssDNA, melting bubbles, and S-DNA during DNA overstretching by single-molecule calorimetry. ***Proc Natl Acad Sci U S A*** 110, 3865-3870 (2013).